LAWRENCE
LIVERMORE
NATIONAL
LABORATORY

LLNL-CONF-405075

Near Infrared Spectroscopy for Burning Plasma Diagnostic Applications

V. A. Soukhanovskii

July 2, 2008

High Temperature Plasma Diagnostics Conference
Albuquerque, NM, United States
May 11, 2008 through May 15, 2008

Disclaimer

Near Infrared Spectroscopy for Burning Plasma Diagnostic Applications *

V. A. Soukhanovskii[1] and NSTX Research Team

[1] *Lawrence Livermore National Laboratory, Livermore, CA*

Abstract

Ultraviolet and visible (UV - VIS, 200-750 nm) atomic spectroscopy of neutral and ion fuel species (H, D, T, Li) and impurities (e.g. He, Be, C, W) is a key element of plasma control and diagnosis on ITER and future magnetically confined burning plasma experiments (BPX). Spectroscopic diagnostic implementation and performance issues that arise in the BPX harsh nuclear environment in the UV-VIS range, e.g., degradation of first mirror reflectivity under charge-exchange atom bombardment (erosion) and impurity deposition, permanent and dynamic loss of window and optical fiber transmission under intense neutron and γ-ray fluxes, are either absent or not as severe in the near-infrared (NIR, 750 - 2000 nm) range. An initial survey of NIR diagnostic applications has been undertaken on the National Spherical Torus Experiment. It is demonstrated that NIR spectroscopy can address machine protection and plasma control diagnostic tasks, as well as plasma performance evaluation and physics studies. Emission intensity estimates demonstrate that NIR measurements are possible in the BPX plasma operating parameter range. Complications in the NIR range due to parasitic background emissions are expected to occur at very high plasma densities, low impurity densities, and at high plasma facing component temperatures.

PACS numbers:

* Contributed paper, published as part of the Proceedings of the 17th Topical Conference on High-Temperature Plasma Diagnostics, Albuquerque, New Mexico, May 2008.

I. INTRODUCTION

Atomic spectroscopy in the ultraviolet (200-400 nm) and visible (400-750 nm) range, referred henceforth as UV-VIS spectroscopy, is one of key elements of plasma control and diagnosis in present and near-future fusion devices, such as the International Thermonuclear Experimental Reactor (ITER) [1, 2]. The UV-VIS spectroscopic applications include detection and analysis of emission from bound-bound and free-bound transitions of neutral atoms and ions of fuel species and impurities, as well as bremsstrahlung emission due to free-free transitions [3]. These emissions come from hot core plasmas, the edge (pedestal) region, and plasma-wall interaction regions (scrape-off layer (SOL), divertors, and limiters). Two main roles are envisioned for UV-VIS spectroscopic diagnostics on ITER and future magnetically-confined fusion (MCF) plasma devices: 1) Machine protection, basic and advanced plasma control applications; and 2) Performance evaluation and physics studies [1, 4, 5].

A harsh nuclear environment of future MCF devices pose severe challenges to spectroscopic diagnostics. In these devices, the diagnostics will be situated in remote locations behind radiation shields. Conceptually, a typical spectroscopic diagnostic is comprised of plasma-facing mirrors, vacuum interface windows, and optical signal relay elements, i.e., mirrors, lenses, optical fibers, situated either in a diagnostic port plug or in a neutron-shielding labyrinth. A detection system can be placed in the port plug with adequate radiation shielding, or in a diagnostic hall adjacent to the shielding labyrinth [6–8].

A significant effort has been dedicated to studying diagnostic requirements in the harsh ITER environment [9]. A reactor-relevant diagnostic experience has been obtained in the DT operation phases of the TFTR and JET tokamaks, as well as in dedicated laboratory irradiation tests [10–12]. These efforts highlighted a number of diagnostic implementation and performance issues for UV-VIS spectroscopy, namely, the severe degradation of optical elements under high plasma particle, neutron, and γ-ray fluxes. An alternative approach proposed here avoids the UV-VIS spectroscopy diagnostic issues.

We propose near-infrared (NIR, 750-2000 nm) spectroscopy as a complementary diagnostic technique for plasma control and performance measurements in the burning plasma experiment (BPX) environment. Whereas the NIR spectroscopic systems share diagnostic concepts with the UV-VIS spectroscopy, optical material and component properties are much more tolerant to radiation and plasma effects in the NIR range, and a number of

NIR signal extraction techniques are available today. Since the BPX diagnostic issues are rarely faced in existing fusion plasma devices, few NIR measurements have been reported [3, 13, 14]. We present an initial study of the scope and feasibility of passive NIR spectroscopic measurements in an ITER-like environment.

II. OPTICAL MATERIALS AND COMPONENTS

Recent diagnostic reviews [2, 9, 12] have summarized the status and requirements for various spectroscopic system components with respect to radiation effects. In ITER, neutron fluxes are expected to be in the range 3×10^{18} m^{-2} s^{-1} at the first wall, the dose rate 2000 Gy s^{-1}, and the neutron heating rate 1 MW m^{-3} [7]. Charge-exchange atomic fluxes with energies up to 1-3 keV are expected to reach 2×10^{19} m^{-2} s^{-1}. The degradation of material properties in this environment is of specific concern for BPX spectroscopic diagnostics, as a number of optical materials and techniques are under consideration for both VIS and NIR measurements. Existing data on first mirror, window and fiber performance under harsh radiation and particle fluxes demonstrate that measurements in the NIR range have clear advantages over those in the UV-VIS range.

a. Mirrors Optical properties of first mirrors, such as reflectivity and polarization, degrade upon exposure of the mirror surface to plasma particle fluxes. Two main mechanisms of surface degradation have been identified - surface erosion and material deposition. Erosion depths and deposition layers of tens of nm are expected in ITER. The specular reflectance is a function of the wavelength λ and mean surface roughness d. The total reflectivity R is described by the Benett formula [15]

$$R = R_0 \, e^{-\frac{(4\pi d)^2}{\lambda^2}} \tag{1}$$

Total reflectivity in the NIR is higher by up to 30 % for the same surface roughness, or alternatively, similar reflectivity degradation in NIR and UV is caused by roughnesses that differ by 80 % in size, according to Eq. 1. Recent tests indicated that mirror heating could prevent or slow down both the erosion and deposition in a deposition-dominated environment, where without heating, the total reflectivity of Mo mirrors was reduced from $\sim$ 60 % to 5-40 % in the UV-VIS range, and from 60-90 % by only 2-10 % in the NIR range [16]. In an erosion-dominated environment, the use of special materials (Mo, W, Rh,

Cu, stainless steel) and manufacturing techniques (single crystal mirrors, polycrystalline mirrors) has been shown to slow down reflectivity degradation in the UV-VIS range. No degradation was detected in the NIR range [17], where high reflectivity coefficients for all candidate mirror materials were predicted and measured.

b. Windows, lenses Radiation-induced damage of bulk optical materials is due to atomic displacement effects and electronic excitation effects. The accumulated damage leads to a permanent optical transmission loss, and is caused by radiation-induced absorption (RIA). The dynamic losses are due to the radiation-induced luminescence (RIL) and Cherenkov radiation. Candidate ITER materials, such as quartz and fused silica, show both RIA and RIL in the UV-VIS range, and no adverse effects in the NIR range. The Cherenkov radiation intensity is an irreducible source of background luminescence. Its intensity decreases rapidly in the NIR range since it is proportional to $1/\lambda^2$ [11].

c. Fibers Optical fibers are considered a more attractive option for signal relay elements than mirrors and lenses because they simplify optical design and alignment procedures, as well as realize significant cost and space savings. Optical fiber materials are also subject to RIA, RIL, and Cherenkov radiation. Key parameters for radiation resistant fibers are dopant elements, OH-content, presence of impurity elements, cladding type, fabrication mechanism, and preconditioning techniques. Recent technology efforts resulted in a number of radiation-resistant fiber candidates with OH-doped and F-doped fused silica SiO_2 cores, as well as mitigation techniques, such as the hydrogen treatment during fabrication and heat treatment [18]. Candidate ITER fiber materials, the KU1 and KS4V types of fused silica, show significant resilience to radiation effects in the VIS range. All spectrally-resolved radiation effect measurements show that these, and other fibers (e.g., quartz, sapphire), are practically free of any RIA and RIL in the NIR range. Finally, an attractive candidate for a fiber-based relay element is the hollow fiber that transmits exclusively in the NIR range [19].

d. Detectors Present day spectroscopic techniques can be used for NIR diagnostics, since instruments and detectors are to be located behind radiation shields. The NIR techniques are conceptually similar to UV-VIS spectroscopy [3], and may include Czerny-Turner spectrometers and filtered photodiode detectors and cameras, build from commercially available components. Since the response of silicon-based charge-coupled devices (CCDs) and photodiodes is limited to below 1100 nm, other detector materials, such as Ge, PbS, InAs,

InGaAs, PbSe, are used in NIR.

III. DIAGNOSTIC SCOPE

A brief review of the UV-VIS spectroscopy issues in the harsh nuclear environment (Section II) demonstrated clear advantages of NIR measurements. Following Ref. [4], we now discuss how NIR spectroscopy can address the diagnostic, plasma control, and machine protection goals envisioned for UV-VIS spectroscopy. The basic tasks include H/D/T-α measurements for ELM and L-H transition monitoring, impurity influx monitoring, and measurements of Z_{eff}. The advanced applications encompass Doppler shift and Doppler broadening spectroscopies, charge-exchange spectroscopy, and Stark broadening spectroscopy for rotation, flow, ion and impurity spicies density $n_{i,Z}$ and temperature T_i profile, effective plasma charge Z_{eff} profile, and divertor T_e, n_e measurements, as well as fuel ratio and neutral density measurements. The proposed NIR measurements are summarized in Table I.

An initial survey of NIR measurements has been performed in the National Spherical Torus Experiment (NSTX), a mid-size mega-Ampere-class fusion plasma device with lithium and carbon plasma facing components (PFCs), up to 6 MW deuterium heating beams, and up to 6 MW of high-harmonic fast wave heating [20]. In the survey, a commercial 0.5 m Czerny-Turner spectrometer equipped with a CCD detector, and a commercial NIR edge filter (Edmunds Optical R72) were used [21]. Both the spectrometer and the fiber-optic imaging system were designed for UV-VIS measurements, thereby limiting the useful wavelength range to about 1150 nm.

A survey spectrum from NSTX lower divertor is shown in Fig. 1. The survey was composed of the spectra taken in five reproducible 0.7 MA, 4 MW NBI-heated discharges. Besides the atomic deuterium Paschen series lines $n = 3 - m$, where $m = 6 - 8$, the lines identified in NSTX spectra are attributed to low-Z impurities. In particular, several bright He I, He II, N I, and O I-II are visible. As for carbon lines, only C I and C III lines were identified. Further tokamak work on line detection and identification in the region is needed. Ionization per photon (SX/B) factors are available in the ADAS system [22] for many of the lines, making them good candidates for particle influx measurements.

While the region $\lambda \leq 910$ nm contains many small atomic and molecular lines, few lines can be seen in the range $\lambda = 910 - 1100$ nm. The line emission-free regions are candidates

for NIR bremsstrahlung measurements for plasma Z_{eff} analysis, as has been shown in Refs. [23, 24], if wall reflections and thermal background emission can be neglected.

To illustrate the complementarity of UV-VIS and NIR measurements, brightness time histories of divertor deuterium Balmer-γ (434 nm) and Paschen-γ (1094 nm) lines are compared in Fig. 2. Both lines were measured in the same divertor region. The visible line was measured with the filterscope [25] consisting of a PMT detector, a narrow-bandpass ($\Delta\lambda =$ 1.5 nm) interference filter, and a 5 kHz bandwidth amplifier. The NIR line was measured with the spectrometer at a CCD framing rate of 25 Hz. Both diagnostics were calibrated in-situ using an integrating sphere calibration transfer standard. A constant low ratio between the two line intensities $R_{B_\gamma/P_\gamma} \simeq 6$ indicates that same atomic processes are responsible for populating the upper levels of these transitions. According to ADAS calculations, the ratios of $R_{B_\gamma/P_\gamma} = 5 - 11$ ($T_e = 1 - 50$ eV) are obtained in ionizing plasmas, and about 2 in recombining plasmas.

Estimates of plasma T_e and n_e in a detached divertor can be obtained from hydrogenic series line emission spectra and photorecombination continuum slope [26]. Substantial Stark broadening ($\lambda/\Delta\lambda \simeq 300$) of the high-$n$ Paschen series lines, due to plasma electron and ion microfields, makes them good candidates for n_e measurements in the range $5 \times 10^{19} - 10^{22}$ m^{-3} [21, 27]. Shown in Fig. 2 are the Paschen P8-P11 NIR lines measured in the recombining divertor in NSTX. Average densities in the range $n_e \simeq 2.5 - 3.5 \times 10^{20}$ m^{-3} were inferred from the Stark broadening analysis of the lines [21].

The discussed examples demonstrate that a number of NIR measurements are possible; however, more work is needed on present day devices to bring the NIR spectroscopy to the level of maturity of the UV-VIS spectroscopy [3].

IV. EMISSION INTENSITY ESTIMATES

Reliable measurements of spectral line intensities and profiles are only possible when the background emission intensity is low. The NIR signal contamination comes from three sources: thermal emission from PFC surfaces, plasma bremsstrahlung emission, and emission due to free-bound transitions (recombination emission). To demonstrate the feasibility of NIR line emission measurements, estimates of line and background intensities are discussed in this section.

Example calculations of the background emission are shown in Fig. 4 (a). In the examples, a line of sight integration of emissivities ϵ through a 1 m isothermal plasma was performed. The bremsstrahlung intensity was estimated using the approach from Ref. [25]. Plasma parameters for these estimates were chosen to determine typical high and low levels of $\epsilon_{brem} \sim n_e^2 Z_{eff} T_e^{-1/2}$. Thermal emission was calculated using the Planck's blackbody emissivity formula. The free-bound hydrogenic intensity was calculated using the CHIANTI suite of codes [28]. Typical line intensities are expected to be in the range 0.01-1000 W m^{-2} nm^{-1}. The thermal emission intensity becomes appreciable only at high PFC temperatures $T \geq$ 1000 K, e.g., in "hot spots" . The free-bound emission intensity can also generally be neglected. The bremstrahlung emission starts competing with line emission only at very high densities and high Z_{eff} levels, marginally achievable in BPX [5]. Overall, it appears that the NIR background intensity at the BPX plasma parameters is sufficiently low to allow reliable line emission measurements.

To provide further comparison of the bremstrahlung and line intensities, we calculated the latter for three candidate NIR lines: hydrogen P$_\alpha$ (λ = 1875.6 nm, $n = 3 - 4$), Be II (λ = 948 nm), and C III (λ = 970.3 nm) using atomic data from the ADAS database [22] (Fig. 4 (b)). These calculations follow the methodology of Ref. [29] where a design for the ITER divertor impurity monitor was evaluated. Line intensities were calculated for a range of T_e, n_e, and divertor particle flux rates expected in ITER. The conclusion for NIR line intensities is similar to the UV-VIS situation [29]: difficulties may be encountered at very high electron densities, where bremstrahlung and free-bound emission become appreciable, and at low recycling and impurity influx levels, where line intensities become low.

V. DISCUSSION

A conceptual evaluation of NIR spectroscopic diagnostic applications in the harsh BPX nuclear environment demonstrate that 1) optical material and component properties under intense neutron, γ-ray, and plasma fluxes favor measurements in the NIR range; and 2) NIR measurements can fully address machine protection, control, and physics studies goals defined for UV-VIS spectroscopy. Intensity estimates demonstrate that NIR measurements are possible in the operating parameter range of BPX plasmas.

To promote the concept of NIR spectroscopic measurements in the BPX environment

further, a number of issues, common to both UV-VIS and NIR diagnostics, still need to be addressed. They include 1) wall reflections (e.g [30]), expected to be higher in the NIR range; 2) molecular band emission, and 3) for graphite PFCs, the background carbon luminescence [31].

Finally, active NIR spectroscopy is an attractive possibility. The motional Stark effect and beam emission spectroscopy measurements are probably not possible in the NIR range, because of a prohibitively large number of deuterium atom states involved at $n = 3, 4$. However, NIR charge-exchange recombination spectroscopy should be considered since a number of suitable transitions between high n levels in highly ionized impurities (He II, Be V, C VI, Ne X) exist.

Acknowledgements Collaboration with Drs R. Kaita and A. L. Roquemore (PPPL) is acknowledged. The entire NSTX team is acknowledged for software, engineering, and technical support, as well as for plasma, NBI and diagnostic operations. ADAS was used through the ORNL Controlled Fusion Atomic Data Center (CFADC). CHIANTI is a collaborative project involving the NRL (USA), RAL (UK), MSSL (UK), the Universities of Florence (Italy) and Cambridge (UK), and George Mason University (USA). This work was performed under the auspices of the U.S. Department of Energy under Contracts W-7405-Eng-48, DE-AC52-07NA27344, and DE-AC02-76CH03073. Prepared by LLNL under Contract DE-AC52-07NA27344.

---

[1] K. Young *et al.*, Nucl. Fusion **39**, 2541 (1999).

[2] A. Donne *et al.*, Nucl. Fusion **47**, 337 (2007).

[3] B. C. Stratton, Fusion Sci. Technol. **53**, 431 (2008).

[4] T. Sugie, A. Costley, A. Malaquias, and C. Walker, J. Plasma Fusion Res. **79**, 1051 (2003).

[5] K. M. Young, Fusion Sci. Technol. **53**, 281 (2008).

[6] C. Walker *et al.*, Fusion Eng. Des. **74**, 685 (2005).

[7] A. E. Costley, T. Sugie, G. Vayakis, and C. I. Walker, Fusion Eng. Des. **74**, 109 (2005).

[8] D. W. Johnson and A. E. Costley, Fusion Sci. Technol. **53**, 751 (2008).

[9] G. Vayakis, E. R. Hodgson, V. Voitsenya, and C. I. Walker, Fusion Sci. Technol. **53**, 699 (2008).

[10] A. Ramsey, Rev. Sci. Instrum. **66**, 871 (1995).

[11] A. C. Maas *et al.*, Fusion Eng. Des. **47**, 247 (1999).

[12] T. Shikama, Nucl. Fusion **43**, 517 (2003).

[13] A. Meigs *et al.*, in *Proc. 27th EPS Conf. on Contr. Fusion and Plasma Phys.* (Budapest, Hungary, 2000), Vol. ECA 24B, pp. 1264–1267.

[14] I. Furno and G. A. Wurden, Rev. Sci. Instrum. **75**, 4112 (2004).

[15] V. Voitsenya *et al.*, Rev. Sci. Instrum **72**, 475 (2001).

[16] D. L. Rudakov, J. A. Boedo, R. A. Moyer, and A. Litnovsky, Rev. Sci. Instrum. **77**, 10F126 (2006).

[17] A. Litnovsky, V. Voitsenya, A. Costley, and A. Donne, Nucl. Fusion **47**, 833 (2007).

[18] M. Decreton, T. Shikama, and E. Hodgson, J. Nuc. Mater. **329**, 125 (2004).

[19] C. M. Smith, N. Venkataraman, M. T. Gallagher, and D. Muller, Nature **424**, 657 (2003).

[20] M. Ono *et al.*, Nucl. Fusion **40**, 557 (2000).

[21] V. A. Soukhanovskii, D. W. Johnson, R. Kaita, and A. Roquemore, Rev. Sci. Instrum. **77**, 10F127 (2006).

[22] H. P. Summers, The ADAS User Manual, version 2.6 **http://adas.phys.strath.ac.uk**, (2004).

[23] K. H. Steuer, H. Rohr, and B. Kurzan, Rev. Sci. Instrum **61**, 3085 (1990).

[24] F. Orsitto *et al.*, Rev. Sci. Instrum **70**, 926 (1999).

[25] A. T. Ramsey and S. L. Turner, Rev. Sci. Instrum. **58**, 1211 (1987).

[26] J. L. Terry *et al.*, Phys. Plasmas **5**, 1759 (1998).

[27] B. Welch *et al.*, AIP Conf. Proc. (USA) **386**, 113 (1997).

[28] E. Landi *et al.*, Astron. Astrophys. Suppl. Ser. **135**, 339 (1999).

[29] T. Sugie *et al.*, Rev. Sci. Instrum. **70**, 351 (1999).

[30] E. M. Hollmann, A. Y. Pigarov, and R. P. Doerner, Rev. Sci. Instrum. **74**, 3984 (2003).

[31] E. Delchambre *et al.*, J. Nucl. Mater. **337-339**, 1069 (2005).

List of Tables

List of Figures

Measurement	NIR Candidate
ELMs, L-H transition	P_α, P_β lines
H,D,T influx and recycling profiles in SOL and divertor	P_α, P_β lines
H / D / T fuel ratio	P_α, P_β lines
Recombination monitoring, T_e and n_e in recombining divertor	Stark broadening of D/T and He I, He II series lines
Divertor and SOL He density	He I, He II lines
Impurity influx and profiles in SOL and divertor	Li, Be, C, N, O lines Ne, Ar, Kr lines W, Mo lines
SOL and divertor flows and passive T_i	Doppler shift and broadening of impurity lines above
Z_{eff}	NIR bremsstrahlung
Corresponding edge measurements	as above

TABLE I: Candidate NIR measurements for BPX machine protection, control, and physics studies

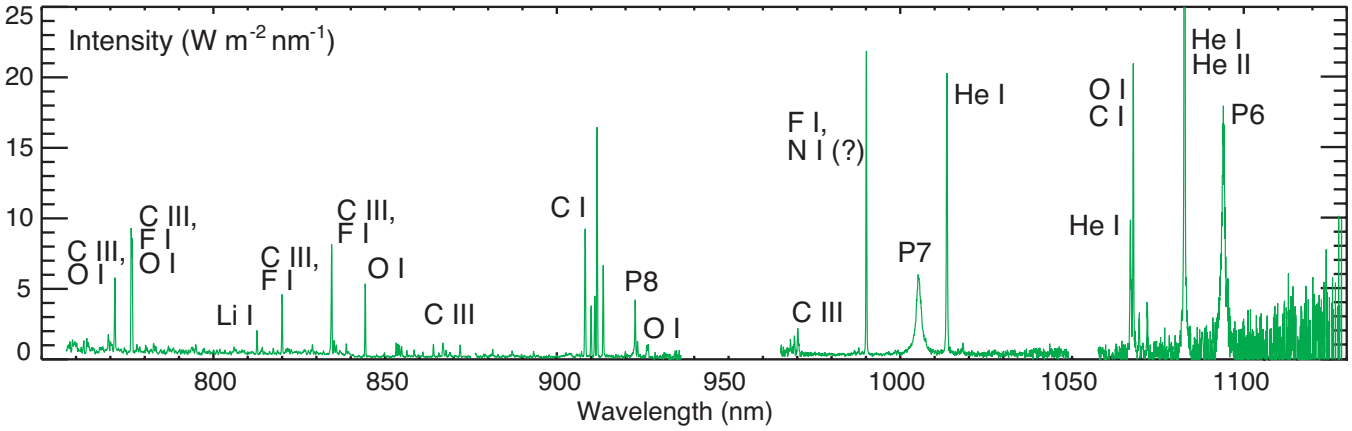

FIG. 1: Survey divertor spectra measured in 0.7 MA, 4 MW NBI-heated NSTX plasmas

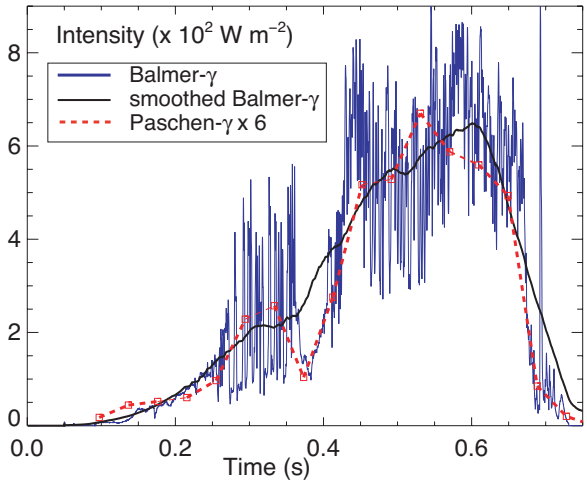

FIG. 2: Time histories of Balmer-γ (2-5) and Paschen-γ (3-6) line intensities in the NSTX divertor.

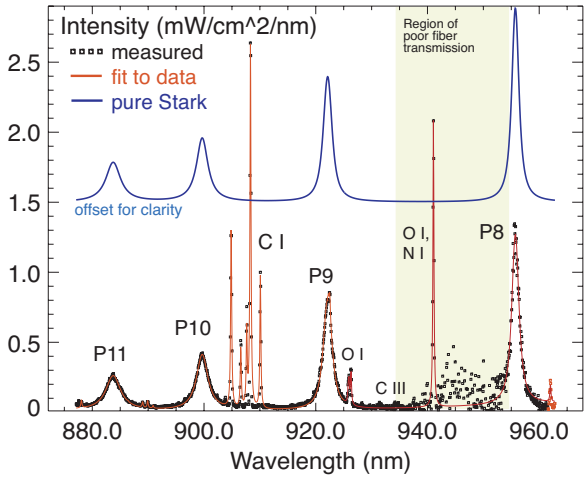

FIG. 3: Stark broadening of P8-P11 Paschen series lines in the recombining (detached) divertor.

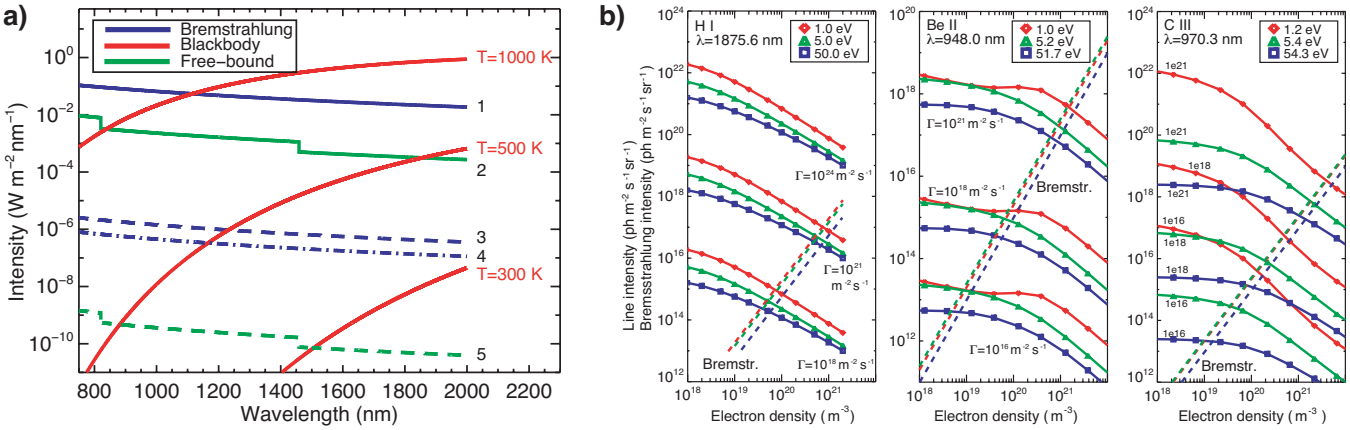

FIG. 4: (a) Near-infrared intensities of thermal (blackbody) emission, bremsstrahlung emission, and free-bound hydrogen emission. Parameters are as follows: lines 1,2 - $T_e = 5$ eV, $n_e = 5 \times 10^{20}$ m^{-3}, $Z_{eff} = 2.5$; lines 3,5 - $T_e = 1000$ eV, $n_e = 1 \times 10^{19}$ m^{-3}, $Z_{eff} = 1.5$; line 4 - $T_e = 10000$ eV, $n_e = 1 \times 10^{19}$ m^{-3}, $Z_{eff} = 1.5$. (b) Line intensities of hydrogen Paschen-α at 1875.6 nm, Be II line at 948.0 nm, and C III line at 970.3 nm as functions of density and particle flux